

# Self-Supervised Transformer with Domain Adaptive Reconstruction for General Face Forgery Video Detection

Daichi Zhang<sup>1,2</sup> Zihao Xiao<sup>3</sup> Jianmin Li<sup>4</sup> Shiming Ge<sup>1,2\*</sup>

<sup>1</sup> Institute of Information Engineering, Chinese Academy of Sciences

<sup>2</sup> School of Cyber Security, University of Chinese Academy of Sciences

<sup>3</sup> RealAI <sup>4</sup> Department of Computer Science and Technology, Tsinghua University

{zhangdaichi, geshiming}@iie.ac.cn, zihao.xiao@realai.ai, lijianmin@mail.tsinghua.edu.cn

## Abstract

Face forgery videos have caused severe social public concern, and various detectors have been proposed recently. However, most of them are trained in a supervised manner with limited generalization when detecting videos from different forgery methods or real source videos. To tackle this issue, we explore to take full advantage of the difference between real and forgery videos by only exploring the common representation of real face videos. In this paper, a **Self-supervised Transformer** cooperating with **Contrastive and Reconstruction learning (CoReST)** is proposed, which is first pre-trained only on real face videos in a self-supervised manner, and then fine-tuned a linear head on specific face forgery video datasets. Two specific auxiliary tasks incorporated contrastive and reconstruction learning are designed to enhance the representation learning. Furthermore, a **Domain Adaptive Reconstruction (DAR)** module is introduced to bridge the gap between different forgery domains by reconstructing on unlabeled target videos when fine-tuning. Extensive experiments on public datasets demonstrate that our proposed method performs even better than the state-of-the-art supervised competitors with impressive generalization.

## 1. Introduction

Face forgery technology has been rapidly developed recently [13, 22, 39, 40, 47, 54, 77], especially after generative adversarial networks (GANs) were proposed [26]. The generated videos can barely be distinguished by the human eye and can be easily produced by accessible online tools, such as Deepfakes<sup>1</sup> and FaceSwap<sup>2</sup>. So an attacker can easily take advantage of these techniques to mislead the public,

\*Corresponding author.

<sup>1</sup><https://github.com/deepfakes/faceswap>

<sup>2</sup><https://github.com/MarekKowalski/FaceSwap>

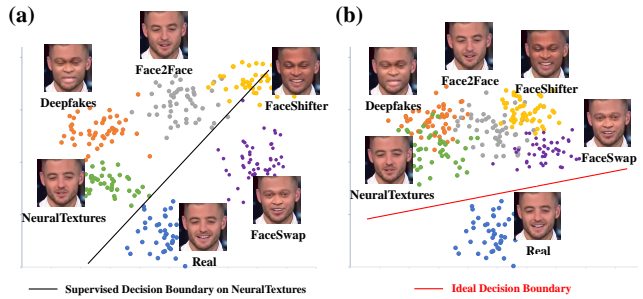


Figure 1. (a) The domain gap exists in real and different forgery face videos. (b) We aim to explore the common representation of real videos in a self-supervised manner and bridge the gap of different forgery domains using unlabeled target domain data.

defame celebrities or even fabricate evidence, leading to serious social, political, and security consequences. To prevent the malicious abuse of face forgery techniques, it is critical to develop effective face forgery video detectors.

Though some existing video-level detectors may achieve considerable performance [1, 36, 50, 60, 86, 91], two major issues still need to be addressed: 1) most of them are trained in a supervised manner, which means large amounts of fake videos with clean annotations are required. 2) we find that real and forgery videos generated from different methods exist domain gaps in latent space, such as Fig. 1 (a) shows, the videos generated from different forgery methods are distinguished in latent space extracted by the Xception trained on FaceForensics++ [67]. And fake videos generated from the same methods but different real source videos could also exhibit differences, such as resolution and illumination differences in source videos. Thus, the supervised detectors trained on specific datasets are poorly generalized and vulnerable. For example, the supervised classification boundary trained on NeuralTextures [76] in Fig. 1 (a) would misclassify the videos generated by FaceShifter [47].

To tackle these two issues, there are two significant insights in our minds. First, with face forgery methods still evolving, it is impossible to train supervised detectors for

unknown forgery methods, but there are massive real face videos in real scenarios. Hence, it may be more appropriate to learn the common representation of real videos rather than overfitting to specific training forgery datasets. Second, since the detector trained on one forgery domain would suffer from domain shift when testing on different forgery domains, but usually unlabeled target domain data is accessible in real scenarios. Noticing we regard fake videos generated from both different forgery methods and source real face videos as different domains. Thus, it would be highly beneficial to leverage unlabeled target domain data to bridge the domain gap. As presented in Fig. 1 (b), we aim to bridge the gap between different domains using unlabeled target domain data and determine the ideal decision boundary by learning the common representation of real face videos.

With all the concerns above in mind, we propose a Self-supervised Transformer cooperating with Contrastive and Reconstruction learning (CoReST) to facilitate face forgery video detection, which includes pre-training and fine-tuning stages. During pre-training, real videos are preprocessed and sampled before being projected into tokens through our designed projector, which are then positionally embedded and fed into our transformer backbone. Contrastive learning and reconstruction learning are introduced to fully explore the common representation of real videos in a self-supervised manner. For contrastive learning, we make the representation learned from the same video closer and different videos far away to explore both intra-video and inter-video representation. For construction learning, a reconstructor is designed to reconstruct the learned video representation into tokens to force the representation retain more spatiotemporal cues of original videos. Then during fine-tuning, we freeze the pre-trained model and fine-tune a linear head on a specific forgery video dataset.

Furthermore, a Domain Adaptive Reconstruction (DAR) module is introduced to bridge the gap between different forgery domains when fine-tuning. Here, we regard fake videos generated from both different forgery methods and real source videos as different domains. Specifically, we add another fully-connected layer before the original linear head and reconstruct the tokens of the unlabeled target domain by the pre-trained reconstructor, forcing the shared representation learn more useful information of the target domain and maintain the discriminability on source domain.

In brief, our contributions are summarized as follows: First, we propose a Self-supervised Transformer cooperating with Contrastive and Reconstruction learning (CoReST) to facilitate face forgery video detection, which is pre-trained only on real videos to explore their common representation with two designed auxiliary tasks, and then fine-tuned a linear head on face forgery video datasets. Second, a Domain Adaptive Reconstruction (DAR) module is introduced to bridge the gap between different face forgery video

domains when fine-tuning. Finally, extensive experiments conducted on public datasets demonstrate the superiority of our proposed method over the state-of-the-art supervised competitors with impressive generalizability.

## 2. Related Work

**Face Forgery Video Detection.** Since face forgery techniques have brought severe threats to society [26], it is urgent to develop forgery detectors. Early detectors focus on hand-crafted features, such as [11, 63] design statistic feature to detect. Recently, variety deep-learning detectors have been proposed, which can be further divided into image-level and video-level detectors. Image-level detectors aim to learn features from cropped facial images to detect, such as [67] choose XceptionNet as backbone and [48] focuses on the blending boundary of forged face. But these methods severely suffer from detecting fake videos. Existing video-level detectors focus more on spatiotemporal cues hiding in forged videos, such as [3, 68, 87, 92]. However, these video-level detectors are trained as naive supervised binary classifiers to learn the specific pattern, which requires large amounts of annotations and suffers a performance drop when detecting videos generated from different forgery methods. We aim to explore the common representation of real face videos and bridge the gap between different forgery types by introducing DAR module.

**Self-Supervised Learning.** Self-supervised learning (SSL) is a subset of unsupervised learning, which automatically generates supervision from the data without labels [16, 25, 38, 61, 89]. The most common strategy for SSL is designing auxiliary pretext tasks to introduce supervised signals, such as reconstruction [27, 33, 65, 84], image colorization [43, 89], image jigsaw puzzle [61], and image inpainting [64]. Contrastive learning has achieved impressive performance on self-supervised representation learning [10, 12, 58, 62, 78, 83], which aims to pull close the positive pairs and push away the negative pairs in latent space. Recent studies have also demonstrated the impressive self-supervised representation capacity of the Vision Transformer (ViT) [2, 6, 19, 45, 91]. There exist some self-supervised detectors, but they focus on specific forgery patterns [9, 50, 72, 88] or the cross-modal mismatch [31, 91], ignoring the intrinsic representation hiding in real face videos. We cooperate vision transformer with two self-supervised tasks: contrastive learning and reconstruction learning to explore the common and intrinsic representation of real videos and distinguish them from fake ones.

**Unsupervised Domain Adaptation.** Unsupervised domain adaptation (UDA) [21] focuses on how to transfer knowledge from a labeled source domain to an unlabeled target domain. Many UDA methods formulate this as a distribution alignment problem, such as [28] computed the Maxi-

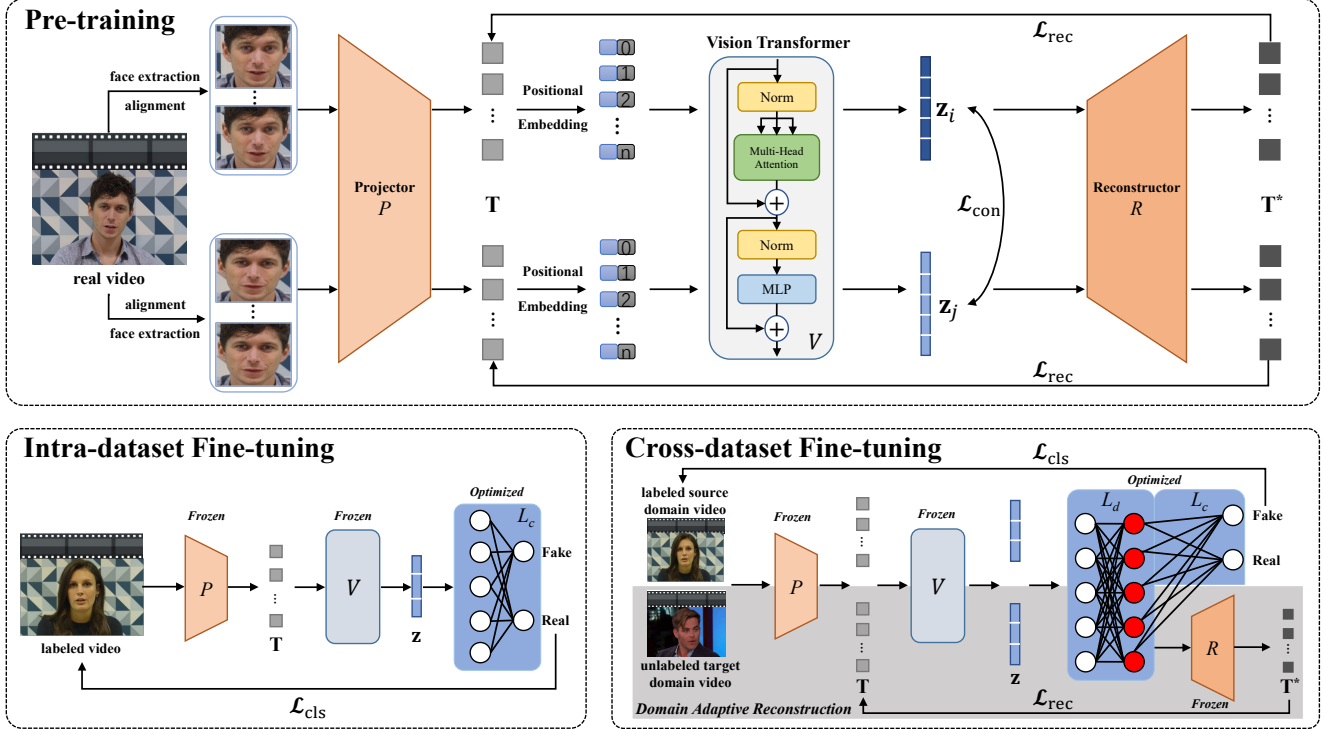


Figure 2. The pipeline of our proposed method. During pre-training, the real videos are first preprocessed by face extraction and alignment, and then projected into token sequence  $\mathbf{T}$  by designed projector  $P$ , which is fed into our transformer backbone  $V$  to extract video representation  $\mathbf{z}$ . The contrastive loss  $\mathcal{L}_{\text{con}}$  and reconstruction loss  $\mathcal{L}_{\text{rec}}$  based on designed reconstructor  $R$  are jointly minimized to train the whole network. During intra-dataset fine-tuning, a linear head  $L_c$  is optimized on labeled forgery datasets with backbone frozen. During cross-dataset fine-tuning, our Domain Adaptive Reconstruction module is introduced by adding an additional linear layer  $L_d$  before  $L_c$  and reconstructing the unlabeled target domain tokens  $\mathbf{T}^*$  through the pre-trained reconstructor  $R$ .

imum Mean Discrepancy (MMD) between source and target domains, and [53] used the Joint MMD criterion to align the joint distributions. Some researchers introduce adversarial learning via a discriminator to judge which domain they are from [35, 52, 80], and others adopt image translation and style transfer for further improvement [4, 59, 70, 73]. There are some existing works that incorporate SSL with UDA methods, such as [23, 24, 41, 75]. In real scenarios, the trained detectors always evaluate unlabeled data from other unknown domains, which can be formulated as a UDA problem. We incorporate SSL with UDA and propose the DAR module to bridge the gap of different forgery domains.

### 3. Proposed Method

In this section, we discuss our proposed method (CoReST) from three aspects: the pre-training stage, the fine-tuning stage, and our Domain Adaptive Reconstruction module, as illustrated in Fig. 2. The following subsections present the details of each part.

#### 3.1. Self-Supervised Pre-training

During the pre-training stage, as presented on the top in Fig. 2, given an input video  $\mathbf{X}$ , we sample clips with

fixed length  $n$  and random offset before employing face detection and alignment to obtain the input frame sequence  $\mathbf{x} = \{f_i\}_{i=1}^n$ . Then, due to the diversity and high dimension of processing video frames, directly pre-training on video frames seems to be expensive. Therefore, to reduce the computational cost, we design a projector  $P(\cdot, \theta_p)$  consisting of convolutional layers to embed each frame into 256 dimensions feature token  $\mathbf{T} = P(\mathbf{x}, \theta_p) = \{\mathbf{t}_i\}_{i=1}^n$  where the dimension of  $\mathbf{t}_i$  is 256. Then the token sequence  $\mathbf{T}$  is reshaped and positional embedded before fed into our naive vision transformer backbone  $V(\cdot, \theta_v)$  to extract representation  $\mathbf{z} = V(\mathbf{T}, \theta_v)$  for each clip. Furthermore, two self-supervised tasks are employed to fully explore the common and intrinsic representation of real face videos, described in detail respectively in the following.

**Contrastive Learning.** We first define the similarity of two different representations  $(\mathbf{z}_i, \mathbf{z}_j)$  extracted by our transformer backbone  $V$ , which can be formulated as follows:

$$\text{sim}(\mathbf{z}_i, \mathbf{z}_j) = \frac{\mathbf{z}_i \cdot \mathbf{z}_j}{\max(\|\mathbf{z}_i\|_2 \cdot \|\mathbf{z}_j\|_2, \epsilon)}, \quad (1)$$

where  $\epsilon$  is set to  $1e - 8$ . Then for a sampled clip  $\mathbf{x}$  with its extracted representation  $\mathbf{z}$ , we consider the representation

extracted from the clips sampled from the same video  $\mathbf{X}$  as positive pairs  $\mathbf{z}^+$ , while those sampled from different videos as negative pairs  $\mathbf{z}^-$ , which could both explore the intra-video and inter-video relations for common real face video representation. Thus, we can formulate the contrastive loss  $\mathcal{L}_{\text{con}}$  within mini-batch samples as follows:

$$\mathcal{L}_{\text{con}} = -\log \frac{\exp(\text{sim}(\mathbf{z}, \mathbf{z}^+) / \tau)}{\exp(\text{sim}(\mathbf{z}, \mathbf{z}^+) / \tau) + \sum \exp(\text{sim}(\mathbf{z}, \mathbf{z}^-) / \tau)}, \quad (2)$$

where the temperature  $\tau$  is set to 0.5. Specifically, for each input video  $\mathbf{X}$ , we sample other clips with the same fixed length  $n$  from a different random offset as positive pairs. Moreover, in each pre-training mini-batch of  $M$  videos, we consider the clips from other  $M-1$  videos as negative pairs, which means there are total  $(M-1) \times M$  negative pairs.

**Reconstruction Learning.** We further introduce a reconstruction pipeline to restore the real face videos, which could force the learned video representation contain more spatiotemporal cues of original real videos. However, since directly reconstructing each frame is too time-consuming and intractable, we aim to reconstruct the embedded token  $\mathbf{t}_i$  of each frame  $f_i$  through a designed reconstructor  $R(\cdot, \theta_r)$  which consists of convolutional layers, to obtain the reconstructed tokens  $\mathbf{T}^* = R(\mathbf{z}, \theta_r) = \{\mathbf{t}_i^*\}_{i=1}^n$ .

During the reconstruction pipeline in pre-training, we compute the reconstruction loss  $\mathcal{L}_{\text{rec}}$  between embedded tokens  $\mathbf{T}$  and reconstructed tokens  $\mathbf{T}^*$ , which can be formulated as follows:

$$\mathcal{L}_{\text{rec}} = \|\mathbf{T}^* - \mathbf{T}\| = \frac{1}{n} \sum_{i=1}^n \|\mathbf{t}_i^* - \mathbf{t}_i\|, \quad (3)$$

where  $n$  is the frame and token sequence length, and we choose  $\ell_1$  norm as our distance function.

Therefore, the total loss function for self-supervised pre-training can be formulated as follows:

$$\mathcal{L}_{\text{ssl}} = \lambda_1 \mathcal{L}_{\text{con}} + \lambda_2 \mathcal{L}_{\text{rec}}, \quad (4)$$

where  $\lambda_1$  and  $\lambda_2$  are the hyper-parameter weights to balance the contrastive and reconstruction loss.

### 3.2. Intra-dataset Fine-tuning

Then during the intra-dataset fine-tuning stage, as presented on the bottom left of Fig. 2, we freeze the parameters of our projector  $\theta_p$  and vision transformer backbone  $\theta_v$  to keep the pre-trained representation capacity of extracting the common representation from real videos. Then, given labeled face forgery video dataset, we fine-tune a one-layer linear head  $L_c$  to predict the possibility of target videos being fake or real. Specifically, we choose the vanilla binary cross-entropy loss  $\mathcal{L}_{\text{cls}} = \mathcal{L}_{\text{bce}}$  to supervise the fine-tuning forgery classification task.

### 3.3. Domain Adaptive Reconstruction

Equipped with the two introduced self-supervised tasks, our proposed CoReST can effectively explore the common representation of real face videos and then fine-tune a linear head to distinguish them from fake ones. However, the gaps between different forgery domains still exist when fine-tuning, which hinders the generalization of the fine-tuned model. Here, we regard both different forgery methods and source real face videos as different domains. But the testing face videos from the unlabeled target domain are easily accessible in real scenarios, even if the forgery method is unknown. To this end, a Domain Adaptive Reconstruction (DAR) module is proposed when fine-tuning to bridge the gap between different forgery domains.

First, we present a brief formulation of *unsupervised domain adaptation* problem. We define a domain as a probability distribution  $\mathcal{D}$  on  $\mathcal{X} \times \mathcal{Y}$ , where  $\mathcal{X}$  is the data space and  $\mathcal{Y}$  is the label space. Then denote the source domain by  $\mathcal{D}_s$  and target domain by  $\mathcal{D}_t$ , where  $\mathcal{D}_s \neq \mathcal{D}_t$ . Given the labeled sample from the source domain  $\mathbf{D}_s = \{(x_s^i, y_s^i)\}_{i=1}^{n_s} \sim \mathcal{D}_s$  and unlabeled sample from the target domain  $\mathbf{D}_t = \{x_t^i\}_{i=1}^{n_t} \sim \mathcal{D}_t^{\mathcal{X}}$ , the objective is to find a function:  $\mathcal{U}_t : \mathcal{X} \rightarrow \mathcal{Y}$  on  $\mathbf{D}_t$  which minimizes the discrepancy between predicted label distribution  $\mathcal{U}_t(\mathbf{D}_t)$  and ground truth label distribution  $\mathcal{D}_t^{\mathcal{Y}}$ . Compared to  $\mathcal{U}_t$ , it is more accessible to find a function:  $\mathcal{U}_s : \mathcal{X} \rightarrow \mathcal{Y}$  on  $\mathbf{D}_s$  through supervised learning. From the perspective of representation learning, the objective is equivalent to finding a function  $\mathcal{O} : \mathcal{X} \rightarrow \mathcal{Z}$ , where  $\mathcal{Z}$  is the latent space, such that the discrepancy between  $\mathcal{D}_s$  and  $\mathcal{D}_t$  is minimized in  $\mathcal{Z}$ . Then we could easily optimize the function  $\mathcal{U} : \mathcal{Z} \rightarrow \mathcal{Y}$  based on the labeled sample from  $\mathcal{D}_s$  in a supervised way.

Thus, the objective is to find the function  $\mathcal{O}$  to bridge the domain gap in latent space, and the function  $\mathcal{U}$  to classify the samples. Based on the formulation above, we hypothesize that the adaptive representation extracted by  $\mathcal{O}$  should satisfy the following two criteria: **(1) accurately classify the sample from the labeled source domain** and **(2) effectively reconstruct the sample from the unlabeled target domain**. The major intuition is that criteria (1) ensure the model maintains its discriminability, and (2) make the shared representation contain more useful information from the target domain. Thus, as shown on the bottom right of Fig. 2, a Domain Adaptive Reconstruction (DAR) module is introduced when fine-tuning by jointly learning a shared representation for two tasks. Specifically, we introduce another linear layer termed domain adaptive layer  $L_d$  before the original linear head  $L_c$ , cooperating with another reconstruction pipeline on the unlabeled target domain. We define  $f_{\text{cls}} : \mathcal{X} \rightarrow \mathcal{Y}$  as the supervised classification pipeline on the labeled source domain, and  $f_{\text{rec}} : \mathcal{X} \rightarrow \mathcal{X}$  as the unsupervised reconstruction pipeline on the unlabeled target



domain, where the  $\mathcal{X}$  is the data space and  $\mathcal{Y}$  is the label space. By optimizing the two pipelines jointly, the representations learned by  $L_d$  from different domains are bridged together, serving as the function  $\tilde{\mathcal{O}}$ , and the classifier  $L_c$  can still effectively classify samples, serving as the function  $\tilde{\mathcal{U}}$ .

Let  $\Theta = \{\Theta_d, \Theta_c\}$  denote the parameters of linear layer  $L_d$  and  $L_c$  respectively. Note that other pre-trained parts of our CoReST are still frozen. We aim to optimize the  $\Theta$  to support both  $f_{\text{cls}}$  and  $f_{\text{rec}}$ . Since directly reconstructing each frame of video is too time-consuming and intractable, we reconstruct the token  $\mathbf{T}$  extracted by our projector  $P(\cdot, \theta_p)$  by  $f_{\text{rec}} : \mathcal{T} \rightarrow \mathcal{T}$ , where  $\mathcal{T}$  is the token space. Given labeled source domain  $\mathbf{D}_s = \{(\mathbf{x}_s^i, \mathbf{y}_s^i)\}_{i=1}^{n_s}$  where  $\mathbf{y}_s^i \in \{0, 1\}$  is the one-hot ground truth label of  $\mathbf{x}_s^i$  being real or fake, and unlabeled target domain  $\mathbf{D}_t = \{(\mathbf{x}_t^i)\}_{i=1}^{n_t}$ , we define the loss functions of the two pipelines below:

$$\mathcal{L}_{\text{cls}}^{n_s}(\{\Theta_d, \Theta_c\}) = \sum_{i=1}^{n_s} \mathcal{L}_{\text{cls}}(f_{\text{cls}}(\mathbf{x}_s^i; \{\Theta_d, \Theta_c\}), \mathbf{y}_s^i), \quad (5)$$

$$\mathcal{L}_{\text{rec}}^{n_t}(\{\Theta_d\}) = \sum_{i=1}^{n_t} \mathcal{L}_{\text{rec}}(f_{\text{rec}}(\mathbf{T}_t^i; \{\Theta_d\}), \mathbf{T}_t^i), \quad (6)$$

where  $\mathbf{T}_t^i$  is the projected token sequence of  $\mathbf{x}_t^i$ ,  $\mathcal{L}_{\text{cls}}$  is the vanilla binary cross-entropy loss  $\mathcal{L}_{\text{bce}}$  and  $\mathcal{L}_{\text{rec}}$  is the reconstruction loss described in Eq. (3). Noticing that the parameters  $\{\Theta_d, \Theta_c\}$  are jointly optimized in  $f_{\text{cls}}$ , while only the  $\Theta_d$  is optimized in  $f_{\text{rec}}$ .

Finally, our goal is to minimize the following objective:

$$\mathcal{L}_{\text{dar}} = \lambda \mathcal{L}_{\text{cls}}^{n_s} + (1 - \lambda) \mathcal{L}_{\text{rec}}^{n_t}, \quad (7)$$

where  $0 \leq \lambda \leq 1$  is a hyper-parameter that controls the trade-off between the supervised classification and unsupervised reconstruction pipelines.

## 4. Experiments

### 4.1. Experimental Settings

**Datasets.** We use two large-scale real face video datasets: VoxCeleb2 [14] and AVSpeech [20] for pre-training. For fine-tuning and evaluation, we choose three widely used face forgery video datasets: FaceForensics++ (FF++) [67], DeepFake Detection Challenge (DFDC) [17], and Celeb-DF(v2) [51]. Specifically, the FF++ dataset contains four subsets generated by different forgery methods: including Deepfakes<sup>3</sup> (DF), Face2Face [77] (F2F), FaceSwap<sup>4</sup> (FS), and NeuralTextures [76] (NT). Unless stated otherwise, we use the mildly compressed version of the dataset (c23). The amount of unlabeled target domain data is 1/10 of the labeled source domain data by random sampling when employing our DAR module during fine-tuning.

<sup>3</sup><https://github.com/deepfakes/faceswap>

<sup>4</sup><https://github.com/MarekKowalski/FaceSwap>

Method	FF++		DFDC		Celeb-DF	
	ACC	AUC	ACC	AUC	ACC	AUC
Xception [67]	95.73	96.30	79.35	89.50	97.90	99.73
MultiAtt [90]	97.60	99.29	76.81	90.32	97.92	99.94
RFM [81]	95.69	98.79	80.83	89.75	97.96	99.94
Add-Net [94]	96.78	97.74	78.71	89.85	96.93	99.55
F <sup>3</sup> -Net [66]	97.52	98.10	76.17	88.39	95.95	98.93
FD <sup>2</sup> -Net [93]	-	99.45	-	66.09	-	-
RECCE [5]	97.06	99.32	81.20	91.33	98.59	99.94
SLADD [9]	-	98.40	-	-	-	79.70
S-MIL-T [49]	84.28	-	85.11	-	98.84	-
TD3denn [86]	79.09	72.22	82.64	78.97	81.08	88.83
STDT [87]	97.97	99.76	97.44	99.14	91.70	97.21
DIANet [36]	96.37	98.80	85.83	90.54	-	-
SBI+EB4 [72]	-	99.64	-	88.70	-	93.74
CoReST (Ours)	<b>99.94</b>	<b>99.99</b>	<b>99.49</b>	<b>99.95</b>	<b>99.61</b>	<b>99.96</b>

Table 1. Intra-dataset comparisons with the state-of-the-art detectors on FF++, DFDC and Celeb-DF datasets. The methods above the line are evaluated at image-level while others are at video-level. Other methods’ results are from their original papers and [5].

**Evaluation Metrics.** To evaluate the performance of our method properly, we report the most commonly used metrics in related arts [1, 5, 48, 67, 85, 90] to compare with prior works, including the Accuracy (ACC(%)), the Area Under the Receiver Operating Characteristic Curve (AUC(%)), the Equal Error Rate (EER(%)) and the F1 (%) score. All metrics are evaluated at video-level unless stated otherwise.

**Implementation Details.** We choose Opencv<sup>5</sup> to extract the frames of all videos and use the face-alignment tool<sup>6</sup> to perform face detection and alignment. We extract clips with continuous 20 frames reshaped into 224×224 for each video from a random offset as input frame sequence. The proposed framework is implemented based on a combination of vanilla CNNs for the projector consisting of three convolutional layers and one average pooling layer, and reconstructor consisting of one convolutional layer, and basic ViT-Base-16 described in [19] for the backbone. We train our model with a batch size of 64, the Adam optimizer with an initial learning rate of 5e−4 and a weight decay of 1e−4. A warm-up scheduler is also employed to adjust the learning rate which is empirically set to 1e−5. We empirically set  $\lambda_1 = 1.0$  and  $\lambda_2 = 0.5$  in Eq. (4). The hyper-parameter weight  $\lambda$  in Eq. (7) is empirically set to 0.5.

### 4.2. Experimental Results

**Intra-dataset Evaluation.** We collect and compare our method with current state-of-the-art detectors on the three datasets. Specifically, for our CoReST, we directly fine-tune the linear head on target forgery video dataset after pre-trained on real videos, and the DAR module is not employed. For fair comparisons, we collect both supervised and self-supervised detectors, such as the MultiAtt [90] and SBI [72], and both image-level and video-level methods, such as the Xception [67] and DIANet [36]. The results are presented in Tab. 1. From the results, our method

<sup>5</sup><https://github.com/opencv/opencv-python>

<sup>6</sup><https://github.com/ladrianb/face-alignment>

Method	DFDC		Celeb-DF	
	AUC↑	EER↓	AUC↑	EER↓
RFM [81]	66.01	39.05	65.63	38.54
MLDG [46]	68.20	37.00	60.90	41.80
LTW [74]	69.00	36.80	64.10	39.70
Add-Net [94]	64.78	40.23	65.29	38.90
F <sup>3</sup> -Net [66]	72.88	33.38	71.21	34.03
MultiAtt [90]	67.34	38.31	76.65	32.83
FFD [15]	69.00	-	76.00	-
GFF [55]	71.58	34.77	75.31	32.48
RECCE [5]	69.06	36.08	68.71	35.73
SLADD [9]	74.20	-	73.00	-
HFI-Net [57]	73.65	-	83.29	-
ICT [18]	-	-	85.71	-
Xception [67]	70.90	-	73.70	-
CNN-aug [82]	72.10	-	75.60	-
Patch-based [8]	65.60	-	69.60	-
Two-branch [56]	-	-	76.70	-
CNN-GRU [69]	68.90	-	69.80	-
Multi-task [60]	68.10	-	75.70	-
DSP-FWA [51]	67.30	-	69.50	-
C3D [79]	61.82	41.52	70.71	33.66
I3D [7]	52.93	48.01	62.45	41.27
BiLSTM [79]	71.24	34.61	72.31	33.53
SIM [29]	68.43	-	77.65	-
X-Ray [48]	65.50	-	79.50	-
LipForensics [32]	73.50	-	82.40	-
HCIL [30]	69.21	-	79.00	-
SST [91]	74.50	-	84.20	-
CoReST (Ours)	72.97	34.05	79.82	26.76
CoReST + DAR (Ours)	<b>74.88</b>	<b>31.45</b>	<b>86.43</b>	<b>20.59</b>

Table 2. Cross-dataset generalization comparisons with the state-of-the-art detectors when trained on FF++ and tested on DFDC and Celeb-DF. The methods above the line are evaluated at image-level while others are at video-level. Other methods’ results are from their original papers and [5, 32, 85].

consistently achieves significant improvements on all three datasets, even better than recent SOTA supervised detectors, such as 9.63% and 22.68% improvements on AUC and ACC compared to MultiAtt [90] on the challenging DFDC dataset, which is the top solution in DFDC competition<sup>7</sup>. Furthermore, our method can still perform better compared to recent self-supervised and video-level detectors, *i.e.*, 6.22% AUC improvement on Celeb-DF compared to recent SBIs [72] and 9.41% AUC improvement on DFDC compared to DIANet [36]. The results demonstrate the effectiveness of our proposed self-supervised method by exploring the common representation of real face videos.

**Generalization Evaluation.** We first conduct cross-dataset experiments by training on FF++ and testing on DFDC and Celeb-DF. Specifically, we report the results when directly fine-tuning and employing the proposed DAR module respectively. The results are presented in Tab. 2. We observe that our CoReST incorporating with DAR module generally outperforms all listed methods on two datasets, *i.e.*, achieving 7.54% and 9.78% AUC improvement compared to supervised MultiAtt [90], 9.38% and 6.93% AUC improvement compared to self-supervised X-Ray [9] on DFDC and Celeb-DF. Furthermore, the directly fine-tuned CoRe-

Approach	Train Dataset	Test Dataset			
		DF	F2F	FS	NT
Xception [67]	DF	99.22	58.81	64.79	59.69
CoReST+DAR		<b>99.75</b>	<b>71.72</b>	<b>70.72</b>	<b>66.79</b>
Xception [67]	F2F	66.39	95.40	56.58	57.59
CoReST+DAR		<b>82.25</b>	<b>99.57</b>	<b>67.78</b>	<b>69.95</b>
Xception [67]	FS	80.00	56.65	94.55	53.42
CoReST+DAR		<b>80.37</b>	<b>64.01</b>	<b>99.81</b>	<b>75.30</b>
Xception [67]	NT	69.94	67.88	57.59	86.72
CoReST+DAR		<b>89.60</b>	<b>80.66</b>	<b>67.44</b>	<b>94.21</b>

Table 3. Cross-manipulation generalization results (video-level AUC(%)) on four subsets of FF++ dataset where trained on one subset and tested on others. The Cross-Avg means the average AUC score on other three subsets except the training subset.

eST can still achieve impressive performance, with 5.63% and 7.47% AUC improvement compared to MultiAtt [90] and X-Ray [9] on DFDC. The DAR module achieves a further AUC improvement by 1.91% and 6.61% on DFDC and Celeb-DF respectively, demonstrating the impressive generalizability of both the proposed CoReST and DAR.

Since the domain gaps refer to differences in both real source videos and manipulation types, we further investigate the cross-manipulation performance of our method, as shown in Tab. 3. We observe that our method still achieves impressive generalization, with average 11.44% AUC improvements compared to Xception [67]. This also indicates the effectiveness and generalization of our method.

### 4.3. Ablation Study

This section analyzes the impact of the pre-training data scale, two self-supervised tasks, the DAR module, and different backbones in both intra- and cross-dataset settings. We freeze the backbone and fine-tune the linear head on FF++ for intra-dataset setting, and employ the DAR module by regarding FF++ as labeled source domain and Celeb-DF as unlabeled target domain for cross-dataset setting.

**Pre-training Data Scale.** We first explore the impact of the number of real face videos used for pre-training. We set the pre-training data scale from 0.0 to 1.0 with an interval of 0.2 and use the ACC and AUC to evaluate the performance, noticing that setting the data scale to 0.0 means there is no pre-training stage and we directly fine-tune the whole network with random initialization. The results are presented in Fig. 3. From the results, we observe that the ACC and AUC in both settings increase with the data scale increasing, and the increase is more significant on cross-dataset evaluation, which demonstrates the effectiveness of our self-supervised method trained on real videos in both intra- and cross-dataset settings.

**Self-supervised Tasks.** We further investigate the impact of two self-supervised tasks (contrastive learning and reconstruction learning) on our model’s performance during pre-training. To evaluate the effectiveness of each task, we conduct ablation studies on each loss function respectively ( $\mathcal{L}_{\text{con}}$  and  $\mathcal{L}_{\text{rec}}$ ). Specifically, we evaluate  $\ell_1$  and  $\ell_2$

<sup>7</sup><https://www.kaggle.com/c/deepfake-detection-challenge/data>

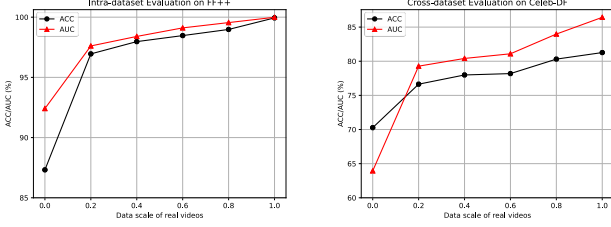


Figure 3. Effect of the pre-training data scales under both intra- and cross-dataset settings.

$\mathcal{L}_{con}$	$\mathcal{L}_{rec1}$	$\mathcal{L}_{rec2}$	FF++		Celeb-DF	
			ACC(%)	AUC(%)	ACC(%)	AUC(%)
✓	-	-	97.96	98.24	75.86	80.37
-	✓	-	98.48	98.74	80.12	84.20
-	-	✓	97.97	98.50	77.61	82.22
✓	✓	-	99.94	99.99	81.27	86.43
✓	-	✓	98.98	99.24	79.34	83.19

Table 4. Analysis of the two self-supervised tasks ( $\mathcal{L}_{con}$  and  $\mathcal{L}_{rec}$ ) during pre-training under both intra- and cross-dataset settings.

distances for reconstruction loss, and we use the same reconstruction loss in pre-training and DAR module. The results are presented in Tab. 4. We find that the performance in both settings declines when removing either reconstruction or contrastive loss, and the  $\ell_1$  reconstruction loss achieves better performance in both settings compared to  $\ell_2$  loss.

**Domain Adaptive Reconstruction.** We evaluate the generalizability of our method when trained on FF++ and tested on DFDC and Celeb-DF in Section 4.2. To further investigate the effectiveness and generalizability of our DAR module, we conduct further ablation studies by training on each of the three datasets and evaluate on the other two with and without the DAR module. The results are shown in Tab. 5. We observe that our proposed CoReST can achieve an impressive generalization under cross-dataset setting and our DAR module can lead to further improvement, with an average 3.66% improvement on ACC, 6.96% improvement on AUC, and 4.31% improvement on EER compared to directly fine-tuning. The results provide more evidence of the improvement in generalization achieved by our proposed DAR module and indicate that our method can properly handle various cross-dataset situations.

**Different Backbones.** We also conduct ablation studies to investigate the ViT backbone’s representation capacity. Specifically, we evaluate on four different ViT backbones: ViT-S16, ViT-S32, ViT-B16 and ViT-B32 [19], and two traditional CNN backbones: ResNet18 and ResNet50 [34]. The results are presented in Tab. 6. We observe that the performance under both settings achieves better when using ViT compared to traditional CNNs, demonstrating the impressive representation capacity of ViT when handling self-supervised tasks. Moreover, the ViT-Base also achieves better performance than ViT-Small, which indicates that the

Fine-tune Set	Test Set	DAR	ACC↑	AUC↑	EER↓
FF++	DFDC	w/o	84.25	72.97	34.05
		w	84.64	74.88	31.45
	Celeb-DF	w/o	77.03	79.82	26.76
		w	81.27	86.43	20.59
DFDC	FF++	w/o	70.05	72.82	31.18
		w	79.19	87.02	20.43
	Celeb-DF	w/o	68.34	66.20	36.47
		w	73.75	74.05	35.01
Celeb-DF	FF++	w/o	85.28	90.74	15.05
		w	87.82	94.95	15.04
	DFDC	w/o	84.25	66.44	38.93
		w	84.51	73.40	34.05

Table 5. Analysis of the proposed DAR module, where we fine-tune on one dataset and evaluate on the other two.

Backbones	FF++		Celeb-DF	
	ACC(%)	AUC(%)	ACC(%)	AUC(%)
ViT-S16	94.42	97.73	73.17	70.79
ViT-S32	90.86	94.33	68.15	61.97
ViT-B16	99.94	99.99	81.27	86.43
ViT-B32	91.37	95.09	71.81	68.45
ResNet18	90.86	95.71	70.66	63.72
ResNet50	92.39	96.11	68.53	62.02

Table 6. Comparisons of ViT-based and CNN-based backbones under both intra- and cross-dataset settings.

Method	DF→F2F	DF→FS	FS→DF	FS→F2F	F2F→FS
FT	65.76	68.92	69.42	66.44	69.21
DAR	<b>68.38</b>	<b>69.62</b>	<b>70.45</b>	<b>66.46</b>	<b>70.71</b>

Table 7. Comparisons with directly fine-tuning (video-level F1 (%)) by regarding different subsets of FF++ as the source and target domains.

Method	CS	CC	BW	GNC	GB	PX	VC	Avg
Xception [67]	99.3	98.6	<b>99.7</b>	53.8	60.2	74.2	62.1	78.3
CNN-aug [82]	99.3	99.1	95.2	54.7	76.5	91.2	72.5	84.1
Patch-based [8]	84.3	74.2	99.2	50.0	54.4	56.7	53.4	67.5
X-Ray [48]	97.6	88.5	99.1	49.8	63.8	88.6	55.2	77.5
CNN-GRU [69]	99.0	98.8	97.9	47.9	71.5	86.5	74.5	82.3
LipForensics [32]	<b>99.9</b>	<b>99.6</b>	87.4	73.8	96.1	95.6	95.6	92.6
FTCN [92]	99.4	96.7	97.1	53.1	95.8	98.2	86.4	89.5
CoReST (Ours)	99.6	99.2	99.1	<b>87.8</b>	<b>98.2</b>	<b>98.8</b>	<b>97.8</b>	<b>97.2</b>

Table 8. Robustness evaluation trained on uncompressed FF++ under seven different perturbations described in [37] (video-level AUC (%)). Other methods’ results are from [31, 32].

ViT model scale also impacts the performance.

#### 4.4. Experimental Analysis

**Directly Fine-tuning.** We make further comparisons with the widely used transfer learning method: directly fine-tuning (FT) to prove the superiority of our method. We use the same backbone with labeled target domain videos for directly fine-tuning after fine-tuning on source domains without layer frozen for 50 epochs. We choose different subsets from FF++ as the source and target domains and the results are presented in Tab. 7. We observe that our method consistently achieves better performance than fine-tuning, which indicates that directly fine-tuning the whole model may lead to limited generalization and the impact of source domain may need more training epochs to eliminate. Moreover, directly fine-tuning on target domain requires labels,

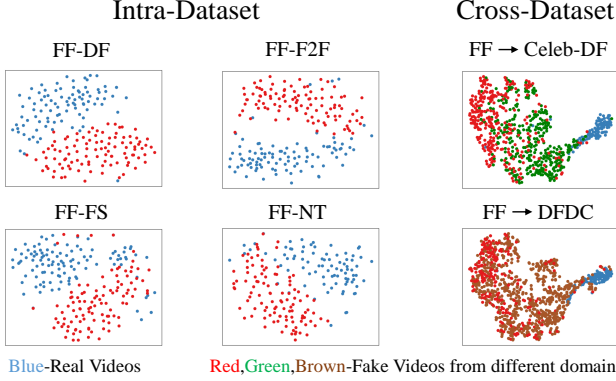


Figure 4. The t-sne [44] visualization of the learned representation under both intra- and cross-dataset settings. The intra-dataset results demonstrate the effectiveness of our self-supervised pre-training by exploring the common representation of real videos, and the cross-dataset results prove our method’s ability to bridge the gap of different forgery domains.

but our method only utilizes unlabeled target domain data.

**Robustness Evaluation.** To evaluate the robustness of our method, we investigate its performance under unseen different perturbations on the FF++ dataset by training on uncompressed videos (raw) but evaluating on videos added perturbations. We consider the following seven perturbations described in [37]: color saturation (CS), color contrast (CC), block-wise (BW), Gaussian noise (GNC), Gaussian blur (GB), pixelation (PX) and video compression (H.264 codec, VC), where each of them has five different severity levels. We report the average AUC scores across five severity levels and make comparisons with existing detectors mentioned above in Tab. 8. We find that our method is more robust than the existing detectors on most of the unseen perturbations, demonstrating its impressive robustness. However, our method is slightly sensitive to block-wise perturbation, which may indicate the intrinsic common representation learned from real face videos is distorted by blocking. Nevertheless, the performance under block-wise perturbation can still achieve a 99.09% AUC score, higher than many existing detectors.

**Representation Visualization.** To evaluate the learned feature distribution of our method, we visualize the video representation learned by our model in both intra- and cross-dataset settings as the same in Sec. 4.3 using t-sne [44]. We visualize the feature extracted from the adaptive layer  $L_d$  for the cross-dataset setting. The results are shown in Fig. 4. From the results, we first observe that the learned representations of real and fake videos are clustered with a clear discrepancy margin in latent space for intra-dataset evaluation, which indicates that our model’s effectiveness by capturing the common representation of real videos to distinguish forged ones. Besides, the fake videos from different datasets are also closely clustered and distinguishable

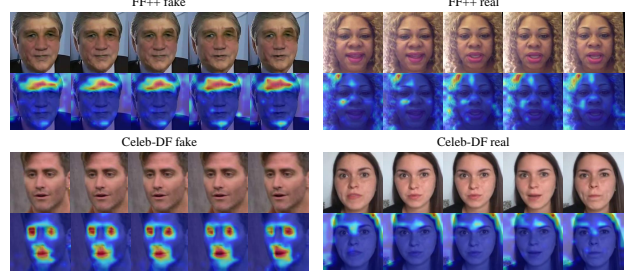


Figure 5. Grad-CAM [71] results under both intra- and cross-dataset settings. We find that our proposed method can effectively respond to the forgery traces in fake videos.

from real videos in latent space for cross-dataset evaluation, which implies that our method effectively bridges the domain gap of different video forgery datasets.

**Explainable Decision.** To better understand the decision-making mechanism of our method, we provide the Grad-CAM [71] heatmaps based on the reconstructed token of each frame in both intra- and cross-dataset settings as the same in Sec. 4.3. The results are shown in Fig. 5. We observe that the heatmap of the forgery data focuses on the specific forgery traces, such as the forehead face boundary in FF++ and the central face area, including eyes and mouth in Celeb-DF. We analyze the difference is caused by the different forgery methods used in FF++ and Celeb-DF datasets. The heatmap for the real data is average on the whole facial area since there are no forgery traces. The results demonstrate the effectiveness of our method from the decision-making perspective and provide human-trustable explanations for decision results.

## 5. Conclusion

In this paper, we propose a Self-supervised Transformer cooperating with Contrastive and Reconstruction learning (CoReST) to facilitate face forgery video detection, which is first pre-trained only on real face videos to explore their common representation with two designed self-supervised tasks and then fine-tuned a linear head on face forgery video dataset. Furthermore, to bridge the gap between videos from different forgery domains, a Domain Adaptive Reconstruction (DAR) module is introduced by reconstructing on the unlabeled target domain videos when fine-tuning. Extensive experiments on public datasets demonstrate the superiority of our method over the state-of-the-art competitors with impressive generalizability. In the future, we intend to further improve our detector’s generalizability in the source-free domain adaptation setting [42] and also apply our proposed method to other media forensic and video understanding tasks.



## References

- [1] Darius Afchar, Vincent Nozick, Junichi Yamagishi, and Isao Echizen. Mesonet: a compact facial video forgery detection network. In *WIFS*, pages 1–7, 2018. 1, 5
- [2] Sara Atito Ali Ahmed, Muhammad Awais, and Josef Kittler. Sit: Self-supervised vision transformer. *CoRR*, abs/2104.03602, 2021. 2
- [3] Irene Amerini and Roberto Caldelli. Exploiting prediction error inconsistencies through lstm-based classifiers to detect deepfake videos. In *IH&MMSec*, pages 97–102, 2020. 2
- [4] Konstantinos Bousmalis, Nathan Silberman, David Dohan, Dumitru Erhan, and Dilip Krishnan. Unsupervised pixel-level domain adaptation with generative adversarial networks. In *CVPR*, pages 95–104, 2017. 3
- [5] Junyi Cao, Chao Ma, Taiping Yao, Shen Chen, Shouhong Ding, and Xiaokang Yang. End-to-end reconstruction-classification learning for face forgery detection. In *CVPR*, pages 4113–4122, 2022. 5, 6
- [6] Mathilde Caron, Hugo Touvron, Ishan Misra, Hervé Jégou, Julien Mairal, Piotr Bojanowski, and Armand Joulin. Emerging properties in self-supervised vision transformers. In *ICCV*, pages 9630–9640, 2021. 2
- [7] João Carreira and Andrew Zisserman. Quo vadis, action recognition? A new model and the kinetics dataset. In *CVPR*, pages 4724–4733, 2017. 6
- [8] Lucy Chai, David Bau, Ser-Nam Lim, and Phillip Isola. What makes fake images detectable? understanding properties that generalize. In *ECCV*, pages 103–120, 2020. 6, 7
- [9] Liang Chen, Yong Zhang, Yibing Song, Lingqiao Liu, and Jue Wang. Self-supervised learning of adversarial example: Towards good generalizations for deepfake detection. In *CVPR*, pages 18689–18698, 2022. 2, 5, 6
- [10] Ting Chen, Simon Kornblith, Mohammad Norouzi, and Geoffrey Hinton. A simple framework for contrastive learning of visual representations. In *ICML*, pages 1597–1607, 2020. 2
- [11] Wen Chen, Yun Q. Shi, and Wei Su. Image splicing detection using 2-d phase congruency and statistical moments of characteristic function. In *Security, Steganography, and Watermarking of Multimedia Contents IX*, page 65050R, 2007. 2
- [12] Xinlei Chen, Haoqi Fan, Ross Girshick, and Kaiming He. Improved baselines with momentum contrastive learning. *arXiv preprint arXiv:2003.04297*, 2020. 2
- [13] Yunjey Choi, Min-Je Choi, Munyoung Kim, Jung-Woo Ha, Sunghun Kim, and Jaegul Choo. Stargan: Unified generative adversarial networks for multi-domain image-to-image translation. In *CVPR*, pages 8789–8797, 2018. 1
- [14] Joon Son Chung, Arsha Nagrani, and Andrew Zisserman. Voxceleb2: Deep speaker recognition. In *Interspeech*, pages 1086–1090, 2018. 5
- [15] Hao Dang, Feng Liu, Joel Stehouwer, Xiaoming Liu, and Anil K. Jain. On the detection of digital face manipulation. In *CVPR*, pages 5780–5789, 2020. 6
- [16] Carl Doersch, Abhinav Gupta, and Alexei A Efros. Unsupervised visual representation learning by context prediction. In *ICCV*, pages 1422–1430, 2015. 2
- [17] Brian Dolhansky, Russ Howes, Ben Pflaum, Nicole Baram, and Cristian Canton Ferrer. The deepfake detection challenge (dfdc) preview dataset. *arXiv preprint arXiv:1910.08854*, 2019. 5
- [18] Xiaoyi Dong, Jianmin Bao, Dongdong Chen, Ting Zhang, Weiming Zhang, Nenghai Yu, Dong Chen, Fang Wen, and Baining Guo. Protecting celebrities with identity consistency transformer. In *CVPR*, pages 9468–9478, 2022. 6
- [19] Alexey Dosovitskiy, Lucas Beyer, Alexander Kolesnikov, Dirk Weissenborn, Xiaohua Zhai, Thomas Unterthiner, Mostafa Dehghani, Matthias Minderer, Georg Heigold, Sylvain Gelly, Jakob Uszkoreit, and Neil Houlsby. An image is worth 16x16 words: Transformers for image recognition at scale. In *ICLR*, 2021. 2, 5, 7
- [20] Ariel Ephrat, Inbar Mosseri, Oran Lang, Tali Dekel, Kevin Wilson, Avinandan Hassidim, William T. Freeman, and Michael Rubinstein. Looking to listen at the cocktail party: a speaker-independent audio-visual model for speech separation. *ACM Trans. Graph.*, 37(4):112, 2018. 5
- [21] Yaroslav Ganin and Victor S. Lempitsky. Unsupervised domain adaptation by backpropagation. In *ICML*, pages 1180–1189, 2015. 2
- [22] Pablo Garrido, Levi Valgaerts, Ole Rehmsen, Thorsten Thormählen, Patrick Pérez, and Christian Theobalt. Automatic face reenactment. In *CVPR*, pages 4217–4224, 2014. 1
- [23] Muhammad Ghifary, W. Bastiaan Kleijn, Mengjie Zhang, and David Balduzzi. Domain generalization for object recognition with multi-task autoencoders. In *ICCV*, pages 2551–2559, 2015. 3
- [24] Muhammad Ghifary, W. Bastiaan Kleijn, Mengjie Zhang, David Balduzzi, and Wen Li. Deep reconstruction-classification networks for unsupervised domain adaptation. In *ECCV*, pages 597–613, 2016. 3
- [25] Spyros Gidaris, Praveer Singh, and Nikos Komodakis. Unsupervised representation learning by predicting image rotations. In *ICLR*, 2018. 2
- [26] Ian J. Goodfellow, Jean Pouget-Abadie, Mehdi Mirza, Bing Xu, David Warde-Farley, Sherjil Ozair, Aaron C. Courville, and Yoshua Bengio. Generative adversarial nets. In *NeurIPS*, pages 2672–2680, 2014. 1, 2
- [27] Ross Goroshin, Joan Bruna, Jonathan Tompson, David Eigen, and Yann LeCun. Unsupervised learning of spatiotemporally coherent metrics. In *ICCV*, pages 4086–4093, 2015. 2
- [28] Arthur Gretton, Karsten M. Borgwardt, Malte J. Rasch, Bernhard Schölkopf, and Alexander J. Smola. A kernel two-sample test. *J. Mach. Learn. Res.*, 13:723–773, 2012. 2
- [29] Zhihao Gu, Yang Chen, Taiping Yao, Shouhong Ding, Jilin Li, and Lizhuang Ma. Delving into the local: Dynamic inconsistency learning for deepfake video detection. In *AAAI*, pages 744–752, 2022. 6
- [30] Zhihao Gu, Taiping Yao, Yang Chen, Shouhong Ding, and Lizhuang Ma. Hierarchical contrastive inconsistency learn-

- ing for deepfake video detection. In *ECCV*, volume 13672, pages 596–613, 2022. 6
- [31] Alexandros Haliassos, Rodrigo Mira, Stavros Petridis, and Maja Pantic. Leveraging real talking faces via self-supervision for robust forgery detection. In *CVPR*, pages 14930–14942, 2022. 2, 7
- [32] Alexandros Haliassos, Konstantinos Vougioukas, Stavros Petridis, and Maja Pantic. Lips don’t lie: A generalisable and robust approach to face forgery detection. In *CVPR*, pages 5039–5049, 2021. 6, 7
- [33] Kaiming He, Xinlei Chen, Saining Xie, Yanghao Li, Piotr Dollár, and Ross B. Girshick. Masked autoencoders are scalable vision learners. In *CVPR*, pages 15979–15988, 2022. 2
- [34] Kaiming He, Xiangyu Zhang, Shaoqing Ren, and Jian Sun. Deep residual learning for image recognition. In *CVPR*, pages 770–778, 2016. 7
- [35] Judy Hoffman, Eric Tzeng, Taesung Park, Jun-Yan Zhu, Phillip Isola, Kate Saenko, Alexei A. Efros, and Trevor Darrell. Cycada: Cycle-consistent adversarial domain adaptation. In *ICML*, pages 1994–2003, 2018. 3
- [36] Ziheng Hu, Hongtao Xie, Yuxin Wang, Jiahong Li, Zhongyuan Wang, and Yongdong Zhang. Dynamic inconsistency-aware deepfake video detection. In *IJCAI*, pages 736–742, 2021. 1, 5, 6
- [37] Liming Jiang, Ren Li, Wayne Wu, Chen Qian, and Chen Change Loy. Deepforensics-1.0: A large-scale dataset for real-world face forgery detection. In *CVPR*, pages 2886–2895, 2020. 7, 8
- [38] Longlong Jing and Yingli Tian. Self-supervised visual feature learning with deep neural networks: A survey. *IEEE Trans. Pattern Anal. Mach. Intell.*, pages 4037–4058, 2020. 2
- [39] Tero Karras, Samuli Laine, and Timo Aila. A style-based generator architecture for generative adversarial networks. In *CVPR*, pages 4401–4410, 2019. 1
- [40] Tero Karras, Samuli Laine, Miika Aittala, Janne Hellsten, Jaakko Lehtinen, and Timo Aila. Analyzing and improving the image quality of stylegan. In *CVPR*, pages 8107–8116, 2020. 1
- [41] Donghyun Kim, Kuniaki Saito, Tae-Hyun Oh, Bryan A. Plummer, Stan Sclaroff, and Kate Saenko. Cross-domain self-supervised learning for domain adaptation with few source labels. *CoRR*, abs/2003.08264, 2020. 3
- [42] Jogendra Nath Kundu, Naveen Venkat, Rahul M. V., and R. Venkatesh Babu. Universal source-free domain adaptation. In *CVPR*, pages 4543–4552, 2020. 8
- [43] Gustav Larsson, Michael Maire, and Gregory Shakhnarovich. Learning representations for automatic colorization. In *ECCV*, pages 577–593, 2016. 2
- [44] Van Der Maaten Laurens and Geoffrey Hinton. Visualizing data using t-sne. *JMLR*, 9(2605):2579–2605, 2008. 8
- [45] Chunyuan Li, Jianwei Yang, Pengchuan Zhang, Mei Gao, Bin Xiao, Xiyang Dai, Lu Yuan, and Jianfeng Gao. Efficient self-supervised vision transformers for representation learning. In *ICLR*, 2022. 2
- [46] Da Li, Yongxin Yang, Yi-Zhe Song, and Timothy M. Hospedales. Learning to generalize: Meta-learning for domain generalization. In *AAAI*, pages 3490–3497, 2018. 6
- [47] Lingzhi Li, Jianmin Bao, Hao Yang, Dong Chen, and Fang Wen. Faceshifter: Towards high fidelity and occlusion aware face swapping. *CoRR*, abs/1912.13457, 2019. 1
- [48] Lingzhi Li, Jianmin Bao, Ting Zhang, Hao Yang, Dong Chen, Fang Wen, and Baining Guo. Face x-ray for more general face forgery detection. In *CVPR*, pages 5001–5010, 2020. 2, 5, 6, 7
- [49] Xiaodan Li, Yining Lang, Yuefeng Chen, Xiaofeng Mao, Yuan He, Shuhui Wang, Hui Xue, and Quan Lu. Sharp multiple instance learning for deepfake video detection. In *ACM MM*, pages 1864–1872, 2020. 5
- [50] Yuezun Li and Siwei Lyu. Exposing deepfake videos by detecting face warping artifacts. In *CVPRW*, pages 46–52, 2019. 1, 2
- [51] Yuezun Li, Xin Yang, Pu Sun, Honggang Qi, and Siwei Lyu. Celeb-DF: A large-scale challenging dataset for deepfake forensics. In *CVPR*, pages 3204–3213, 2020. 5, 6
- [52] Mingsheng Long, Zhangjie Cao, Jianmin Wang, and Michael I. Jordan. Conditional adversarial domain adaptation. In *NeurIPS*, pages 1647–1657, 2018. 3
- [53] Mingsheng Long, Han Zhu, Jianmin Wang, and Michael I. Jordan. Deep transfer learning with joint adaptation networks. In *ICML*, pages 2208–2217, 2017. 3
- [54] Yongyi Lu, Yu-Wing Tai, and Chi-Keung Tang. Attribute-guided face generation using conditional cyclegan. In *ECCV*, pages 293–308, 2018. 1
- [55] Yuchen Luo, Yong Zhang, Junchi Yan, and Wei Liu. Generalizing face forgery detection with high-frequency features. In *CVPR*, pages 16317–16326, 2021. 6
- [56] Iacopo Masi, Aditya Killekar, Royston Marian Mascarenhas, Shenoy Pratik Gurudatt, and Wael AbdAlmageed. Two-branch recurrent network for isolating deepfakes in videos. In *ECCV*, pages 667–684, 2020. 6
- [57] Changtao Miao, Zichang Tan, Qi Chu, Nenghai Yu, and Guodong Guo. Hierarchical frequency-assisted interactive networks for face manipulation detection. *IEEE Trans. Inf. Forensics Secur.*, 17:3008–3021, 2022. 6
- [58] Ishan Misra and Laurens van der Maaten. Self-supervised learning of pretext-invariant representations. In *CVPR*, pages 6707–6717, 2020. 2
- [59] Zak Murez, Soheil Kolouri, David J. Kriegman, Ravi Ramamoorthi, and Kyungnam Kim. Image to image translation for domain adaptation. In *CVPR*, pages 4500–4509, 2018. 3
- [60] Huy H Nguyen, Fuming Fang, Junichi Yamagishi, and Isao Echizen. Multi-task learning for detecting and segmenting manipulated facial images and videos. In *BTAS*, pages 1–8, 2019. 1, 6
- [61] Mehdi Noroozi and Paolo Favaro. Unsupervised learning of visual representations by solving jigsaw puzzles. In *ECCV*, pages 69–84, 2016. 2
- [62] Aaron van den Oord, Yazhe Li, and Oriol Vinyals. Representation learning with contrastive predictive coding. *arXiv preprint arXiv:1807.03748*, 2018. 2
- [63] Xunyu Pan, Xing Zhang, and Siwei Lyu. Exposing image splicing with inconsistent local noise variances. In *ICCP*, pages 1–10, 2012. 2

- [64] Deepak Pathak, Philipp Krahenbuhl, Jeff Donahue, Trevor Darrell, and Alexei A Efros. Context encoders: Feature learning by inpainting. In *CVPR*, pages 2536–2544, 2016. [2](#)
- [65] Viorica Patraucean, Ankur Handa, and Roberto Cipolla. Spatio-temporal video autoencoder with differentiable memory. *arXiv preprint arXiv:1511.06309*, 2015. [2](#)
- [66] Yuyang Qian, Guojun Yin, Lu Sheng, Zixuan Chen, and Jing Shao. Thinking in frequency: Face forgery detection by mining frequency-aware clues. In *ECCV*, pages 86–103, 2020. [5, 6](#)
- [67] Andreas Rössler, Davide Cozzolino, Luisa Verdoliva, Christian Riess, Justus Thies, and Matthias Nießner. Faceforensics++: Learning to detect manipulated facial images. In *ICCV*, pages 1–11, 2019. [1, 2, 5, 6, 7](#)
- [68] Ekraam Sabir, Jiaxin Cheng, Ayush Jaiswal, Wael AbdAlmageed, Iacopo Masi, and Prem Natarajan. Recurrent convolutional strategies for face manipulation detection in videos. In *CVPRW*, pages 80–87, 2019. [2](#)
- [69] Ekraam Sabir, Jiaxin Cheng, Ayush Jaiswal, Wael AbdAlmageed, Iacopo Masi, and Prem Natarajan. Recurrent convolutional strategies for face manipulation detection in videos. In *CVPRW*, pages 80–87, 2019. [6, 7](#)
- [70] Swami Sankaranarayanan, Yogesh Balaji, Carlos Domingo Castillo, and Rama Chellappa. Generate to adapt: Aligning domains using generative adversarial networks. In *CVPR*, pages 8503–8512, 2018. [3](#)
- [71] Ramprasaath R. Selvaraju, Michael Cogswell, Abhishek Das, Ramakrishna Vedantam, Devi Parikh, and Dhruv Batra. Grad-cam: Visual explanations from deep networks via gradient-based localization. In *ICCV*, pages 618–626, 2017. [8](#)
- [72] Kaede Shiohara and Toshihiko Yamasaki. Detecting deepfakes with self-blended images. In *CVPR*, pages 18699–18708, 2022. [2, 5, 6](#)
- [73] Ashish Shrivastava, Tomas Pfister, Oncel Tuzel, Joshua Susskind, Wenda Wang, and Russell Webb. Learning from simulated and unsupervised images through adversarial training. In *CVPR*, pages 2242–2251, 2017. [3](#)
- [74] Ke Sun, Hong Liu, Qixiang Ye, Yue Gao, Jianzhuang Liu, Ling Shao, and Rongrong Ji. Domain general face forgery detection by learning to weight. In *AAAI*, pages 2638–2646, 2021. [6](#)
- [75] Yu Sun, Eric Tzeng, Trevor Darrell, and Alexei A. Efros. Unsupervised domain adaptation through self-supervision. *CoRR*, abs/1909.11825, 2019. [3](#)
- [76] Justus Thies, Michael Zollhöfer, and Matthias Nießner. Deferred neural rendering: image synthesis using neural textures. *ACM TOG*, 38(4):66:1–12, 2019. [1, 5](#)
- [77] Justus Thies, Michael Zollhofer, Marc Stamminger, Christian Theobalt, and Matthias Nießner. Face2face: Real-time face capture and reenactment of rgb videos. In *CVPR*, pages 2387–2395, 2016. [1, 5](#)
- [78] Yonglong Tian, Dilip Krishnan, and Phillip Isola. Contrastive multiview coding. In *ECCV*, pages 776–794, 2020. [2](#)
- [79] Du Tran, Lubomir D. Bourdev, Rob Fergus, Lorenzo Torresani, and Manohar Paluri. Learning spatiotemporal features with 3d convolutional networks. In *ICCV*, pages 4489–4497, 2015. [6](#)
- [80] Eric Tzeng, Judy Hoffman, Kate Saenko, and Trevor Darrell. Adversarial discriminative domain adaptation. In *CVPR*, pages 2962–2971, 2017. [3](#)
- [81] Chengrui Wang and Weihong Deng. Representative forgery mining for fake face detection. In *CVPR*, pages 14923–14932, 2021. [5, 6](#)
- [82] Sheng-Yu Wang, Oliver Wang, Richard Zhang, Andrew Owens, and Alexei A Efros. CNN-generated images are surprisingly easy to spot... for now. In *CVPR*, pages 8695–8704, 2020. [6, 7](#)
- [83] Xiaolong Wang and Abhinav Gupta. Unsupervised learning of visual representations using videos. In *ICCV*, pages 2794–2802, 2015. [2](#)
- [84] Zhenda Xie, Zheng Zhang, Yue Cao, Yutong Lin, Jianmin Bao, Zhuliang Yao, Qi Dai, and Han Hu. Simsim: A simple framework for masked image modeling. In *CVPR*, pages 9653–9663, 2022. [2](#)
- [85] Xiao Yang, Shilong Liu, Yinpeng Dong, Hang Su, Lei Zhang, and Jun Zhu. Towards generalizable detection of face forgery via self-guided model-agnostic learning. *Pattern Recognit. Lett.*, pages 98–104, 2022. [5, 6](#)
- [86] Daichi Zhang, Chenyu Li, Fanzhao Lin, Dan Zeng, and Shiming Ge. Detecting Deepfake Videos with Temporal Dropout 3DCNN. In *IJCAI*, pages 1288–1294, 2021. [1, 5](#)
- [87] Daichi Zhang, Fanzhao Lin, Yingying Hua, Pengju Wang, Dan Zeng, and Shiming Ge. Deepfake video detection with spatiotemporal dropout transformer. In *ACM MM*, pages 5833–5841, 2022. [2, 5](#)
- [88] Jian Zhang, Jiangqun Ni, and Hao Xie. Deepfake videos detection using self-supervised decoupling network. In *ICME*, pages 1–6, 2021. [2](#)
- [89] Richard Zhang, Phillip Isola, and Alexei A Efros. Colorful image colorization. In *ECCV*, pages 649–666, 2016. [2](#)
- [90] Hanqing Zhao, Wenbo Zhou, Dongdong Chen, Tianyi Wei, Weiming Zhang, and Nenghai Yu. Multi-attentional deepfake detection. In *CVPR*, pages 2185–2194, 2021. [5, 6](#)
- [91] Hanqing Zhao, Wenbo Zhou, Dongdong Chen, Weiming Zhang, and Nenghai Yu. Self-supervised transformer for deepfake detection. *CoRR*, abs/2203.01265, 2022. [1, 2, 6](#)
- [92] Yinglin Zheng, Jianmin Bao, Dong Chen, Ming Zeng, and Fang Wen. Exploring temporal coherence for more general video face forgery detection. In *ICCV*, pages 15024–15034, 2021. [2, 7](#)
- [93] Xiangyu Zhu, Hao Wang, Hongyan Fei, Zhen Lei, and Stan Z Li. Face forgery detection by 3d decomposition. In *CVPR*, pages 2929–2939, 2021. [5](#)
- [94] Bojia Zi, Minghao Chang, Jingjing Chen, Xingjun Ma, and Yu-Gang Jiang. Wilddeepfake: A challenging real-world dataset for deepfake detection. In *ACM MM*, pages 2382–2390, 2020. [5, 6](#)